Fast Neutron Detection Using Pixelated CdZnTe Spectrometers

Michael Streicher, David Goodman, Yuefeng Zhu, Steven Brown, Scott Kiff, and Zhong He, *Senior Member, IEEE*

***Abstract*— Fast neutrons are an important signature of special nuclear materials (SNMs). They have a low natural background rate and readily penetrate high atomic number materials that easily shield gamma-ray signatures. Therefore, they provide a complementary signal to gamma rays for detecting shielded SNM. Scattering kinematics dictate that a large nucleus (such as Cd or Te) will recoil with small kinetic energy after an elastic collision with a fast neutron. Charge carrier recombination and quenching further reduce the recorded energy deposited. Thus, the energy threshold of CdZnTe detectors must be very low in order to sense the small signals from these recoils. In this paper, the threshold was reduced to less than 5 keVee to demonstrate that the 5.9-keV X-ray line from ^{55}Fe could be separated from electronic noise. Elastic scattering neutron interactions were observed as small energy depositions (less than 20 keVee) using digitally sampled pulse waveforms from pixelated CdZnTe detectors. Characteristic gamma-ray lines from inelastic neutron scattering were also observed.**

***Index Terms*— CdZnTe detectors, gamma-ray spectroscopy, low-energy threshold systems, neutron detectors, special nuclear materials (SNMs) monitoring.**

I. Introduction

SPECIAL NUCLEAR MATERIAL (SNM) emits high-energy neutrons following spontaneous fission or during active interrogation with a neutron or a high-energy photon source [1]. The emitted neutrons will follow a Watt distribution with the most probable neutron energy around 1 MeV and a mean energy of 2 MeV. Fast neutrons are rare in the natural background with a flux of only $1.8 \pm 0.2 \times 10^{-3}$ cm$^{-2}s^{-1}$ at sea level [2] (although some have measured higher rates [3]), so they are a useful signature for detecting SNM. Unlike gamma rays, fission-energy neutrons are not easily shielded and can escape high atomic number shielding materials without significant attenuation. Therefore, fast neutrons provide a complementary signal to gamma rays for detection of shielded SNM.

Thermal neutrons are easier to detect than fast neutrons because the interaction cross sections are significantly higher. Many thermal neutron detectors have been developed based on ^{10}B, ^{7}Li, and most notably, ^{3}He reactions. The production of a charged particle from a high-Q value reaction makes detection straightforward. (n, γ) reactions have also been used to detect thermal neutrons, even using CdTe [4] or CdZnTe as the conversion layer [5], [6].

Often, fast neutrons are detected by first thermalizing them through scattering interactions in a moderator. Then the initially fast neutrons are detected via thermal neutron interactions. However, by thermalizing the neutrons, information about the incident neutron energy spectrum is lost. A neutron energy spectrum can be useful to discriminate different types of neutron sources. Also, by estimating the energies of neutron scatterings, one can image neutron sources using scattering kinematics [7]. Low-Z scintillating material with good neutron-photon pulse shaped discrimination has long been employed to estimate the neutron energy spectrum after spectrum unfolding [8], [9].

Semiconductor detectors such as high-purity germanium (HPGe) have been used to study elastically and inelastically scattered neutrons [10], [11]. Like HPGe, CdZnTe detection systems provide high-resolution gamma-ray spectroscopy and imaging, but add the convenience of room-temperature operation. In national security applications, a sensor that can characterize shielding materials and determine isotopic composition of SNM (as CdZnTe can [12], [13]) while providing gamma-ray imaging and simultaneously detecting both fast and thermal neutrons in a rapidly deployable package could be quite valuable. CdZnTe can serve as a thermal neutron detector via capture on ^{113}Cd and detection of gamma-rays from the cascade following capture. This paper will demonstrate how CdZnTe can serve as a fast neutron detector via direct detection of elastic scattering or detection of gamma rays following inelastic scattering.

The CdZnTe array system used in this paper consisted of four $2 \times 2 \times 1.5$ cm^3 3-D position-sensitive CdZnTe gamma-ray detectors. Each detector was read out by a VAD_UMv1.2 ASIC developed jointly by the University of Michigan and Integrated Detector Electronics AS (Oslo, Norway) [14]. The system demonstrated an energy resolution of 0.47% full-width at half-maximum (FWHM) at 662 keV for single pixel events and 0.63% FWHM at 662 keV for all events [15].

II. Detection Signatures and Theoretical Efficiency

At high energies, neutrons primarily interact with CdZnTe target nuclei through inelastic or elastic scattering [16].

Manuscript received January 17, 2017; revised March 21, 2017 and April 18, 2017; accepted May 3, 2017. Date of publication May 29, 2017; date of current version July 14, 2017. This work was supported in part by DOD DTRA through the National Science Foundation Graduate Research Fellowship under Award HDTRA1-12-C-0034 and in part by the U.S. Department of Energy's National Nuclear Security Administration under Contract DE-NA0003525.

M. Streicher, D. Goodman, Y. Zhu, S. Brown, and Z. He are with the Department of Nuclear Engineering and Radiological Sciences, University of Michigan, Ann Arbor, MI 48109 USA (e-mail: streichm@umich.edu).

S. Kiff is with Sandia National Laboratories, Livermore, CA 94550 USA.

Color versions of one or more of the figures in this paper are available online at http://ieeexplore.ieee.org.

Digital Object Identifier 10.1109/TNS.2017.2709543

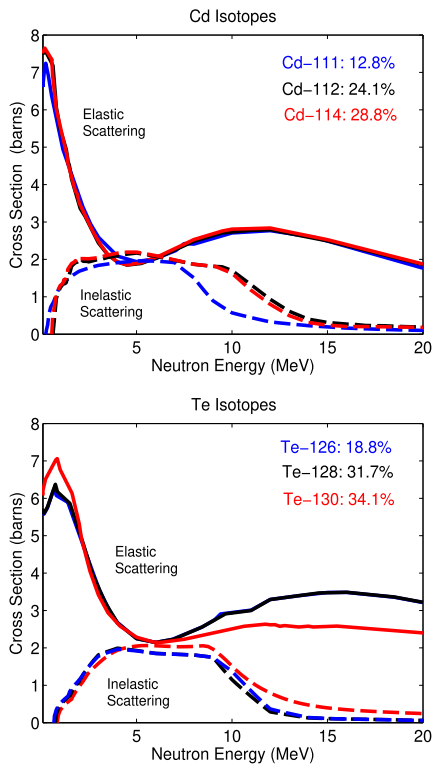

Fig. 1. Microscopic cross sections for neutron interactions on Cd or Te nuclei. The dashed lines indicate the cross section for inelastic scattering, whereas the solid lines indicate the cross section for elastic scattering. The three most abundant isotopes are plotted for each element, but the minor isotopes follow the same trends.

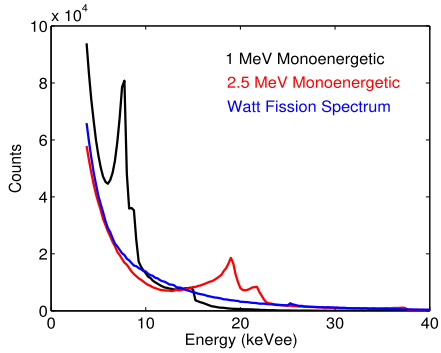

Fig. 2. Simulated elastic scattering recoil energy spectra from various neutron sources in CdZnTe detectors. These data were simulated in Geant4 [22], assuming a quenching factor of 0.25. The spectra are cutoff at 4 keVee. Ten million incident neutrons were simulated for each spectrum, so the relative number of counts reflects the detection efficiency.

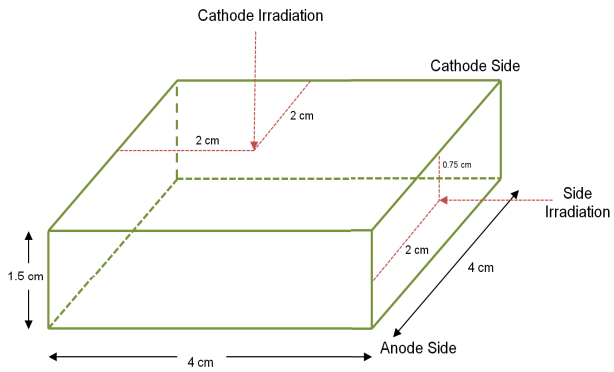

Fig. 3. Sketch of simulated neutron beams incident on CdZnTe to estimate intrinsic efficiency.

Inelastically scattered neutrons do impart some recoil energy to the target nucleus while producing characteristic gamma rays depending on the nuclear levels of the target. If these gamma-ray lines can be efficiently detected and separated from background, they indicate fast neutron reactions.

The energy deposited by an elastically scattered neutron to the recoil nucleus E_r depends on the incident neutron energy E_n, the scattering angle between the incident and scattered neutrons in the center-of-mass frame of reference θ_c, and the target nucleus mass A, as [17]

$$E_r = E_n \left(1 - \frac{(1+\alpha) + (1-\alpha)\cos\theta_c}{2}\right) \quad (1)$$

$$\alpha \equiv \left(\frac{A-1}{A+1}\right)^2. \quad (2)$$

Since the primary constituent nuclei of CdZnTe detectors are one hundred times more massive than the neutron, E_r is small, even for backscattered events (when $\cos(\theta_c) \approx -1$) because α is close to one. Backscattering on Cd or Te will deposit less than 4% of the incident neutron energy to the recoil nucleus.

The microscopic cross sections for fast neutron interactions in Cd and Te nuclei are shown in Fig. 1. For both elements, the cross section for scattering is a few barns, with elastic collisions being more likely at most energies.

The recorded energy will be reduced further due to quenching. Nuclear recoils will generate fewer electron-hole pairs than the number produced by a photoelectron of the same energy [18]. This process can be described via the Lindhard model [19]. The quenching factor for CdZnTe is estimated to be 25% based on previous work with neutron scattering in silicon and germanium [20], [21], which both exhibit quenching factors of about 25% for 50-keV recoil nuclei.

Assuming a quenching factor of 0.25, simulated neutron energy spectra recorded using CdZnTe are shown in Fig. 2. Ten million neutrons are simulated for each neutron source. These spectra do not include the 2-keV Gaussian blur from electronic noise expected from a real system.

In a Geant4 [22] simulation, neutron beams of three different energy distributions were directed at the center of the cathode side or the center of the side of the detector array as illustrated in Fig. 3. The detector array was simulated as one large detector. The efficiency was calculated as the number of quenched nuclear recoils above the low-energy threshold divided by the simulated number of neutrons in the beam (ten million neutrons). The elastic nuclear recoil theoretical detection efficiency from these simulations is summarized in Table I. Overall, the intrinsic efficiency is of the order of a few percent and is strongly dependent on the low-energy threshold. Since the number of simulated particles was large, the uncertainty in the simulated detection efficiency is less than 0.1% in absolute terms.

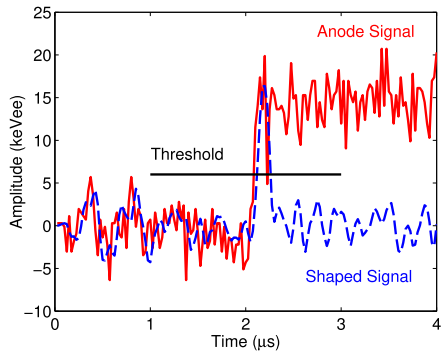

Fig. 4. Example pulse waveform and filtered signal for a small-energy gamma-ray deposition. The waveform is sampled at 40 MHz.

TABLE I

SIMULATED INTRINSIC EFFICIENCY OF A PROTOTYPE CdZnTe ARRAY SYSTEM READ OUT BY ASICs, WHICH DIGITALLY SAMPLES THE PULSE WAVEFORMS TO NEUTRONS FOR DIFFERENT BEAM GEOMETRIES, LOW-ENERGY THRESHOLDS, AND NEUTRON ENERGIES IN GEANT4

Neutron Energy	Low-Energy Threshold	Irradiation Direction	Detection Efficiency (%)
1 MeV	5 keVee	Side	11.3
1 MeV	10 keVee	Side	2.2
2.5 MeV	5 keVee	Side	9.0
2.5 MeV	10 keVee	Side	4.9
Watt Spectrum	5 keVee	Side	8.1
Watt Spectrum	10 keVee	Side	3.5
1 MeV	5 keVee	Cathode	4.9
1 MeV	10 keVee	Cathode	0.9
2.5 MeV	5 keVee	Cathode	3.6
2.5 MeV	10 keVee	Cathode	2.0
Watt Spectrum	5 keVee	Cathode	3.3
Watt Spectrum	10 keVee	Cathode	1.4

III. LOW-ENERGY THRESHOLDS IN PIXELATED CdZnTe DETECTORS

To trigger the VAD_UMv1.2 ASIC, a filtered signal induced on an anode pixel must exceed a user-defined threshold. A CR-$(RC)^4$ filter with a short shaping time is employed by the triggering logic. First, a global threshold is found based on the lowest setting where noise triggering barely saturates the system. Then, each channel is enabled individually to see if that channel contributes significantly to the number of triggers from noise. If the channel does not exhibit a superfluous noise trigger rate, the global threshold is trimmed slightly lower on a channel-by-channel basis until noise triggers become predominant. If the channel does contribute significantly to the number of noise triggers, the threshold is raised slightly higher. Using this procedure, the threshold can be lowered to around 5 keVee with a false trigger rate of less than one count per second. Fig. 4 demonstrates what low amplitude signals look like read out by the VAD_UMv1.2 system. The threshold will vary slightly from channel to channel. Edge pixels tend to have higher energy thresholds (around 10 keVee) due to leakage current from the pixel to the guard ring.

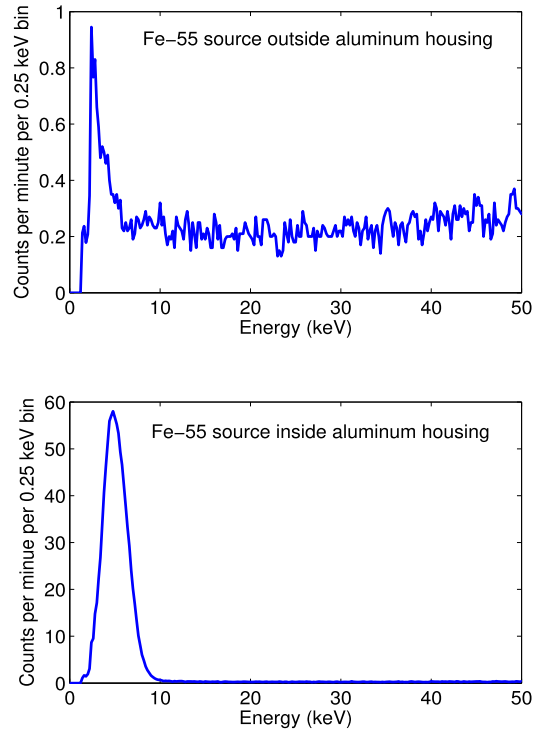

Fig. 5. Recorded energy spectrum from a 1.5 μCi ^{55}Fe source with the source outside of the detector housing box (top) and inside the housing (bottom). Each configuration was measured for 1 h.

Transient signals [23], [24] induced on pixels neighboring the pixel that collects the charge can also trigger the system using this triggering logic. In order to accurately discriminate transient signals from pixels that collect charge, a software threshold is employed. The mean amplitude of the first fifty digitally sampled points is subtracted from the mean value of the last fifty sample points to estimate the pulse amplitude. This amplitude should be above a few keV for collecting pixels. If the amplitude is lower than the software threshold, the trigger is reclassified as a transient signal.

With the low-energy threshold at around 5 keV, the X-rays from a ^{55}Fe source at 5.9 keV can easily be distinguished from noise as shown in Fig. 5. The source must be placed inside the detector housing, as the 2-mm-thick aluminum box provides substantial attenuation to low-energy photons. With the source outside the aluminum housing, the continuum to the right of the peak is caused by low-energy background photons that are not attenuated by the aluminum housing or higher energy background gammas that undergo small-angle Compton scattering in the detector. The peak at very low energies is a convolution of some noise triggering and some 5.9-keV source photons that are not attenuated by the aluminum detector housing. With the source inside the housing, the low-energy peak is primarily from photoelectrically absorbed 5.9-keV photons from the ^{55}Fe source. The electronic noise component is still present, but is weak relative to the source strength.

Because the detector housing attenuates a significant fraction of low-energy photons, an alternative method to measure

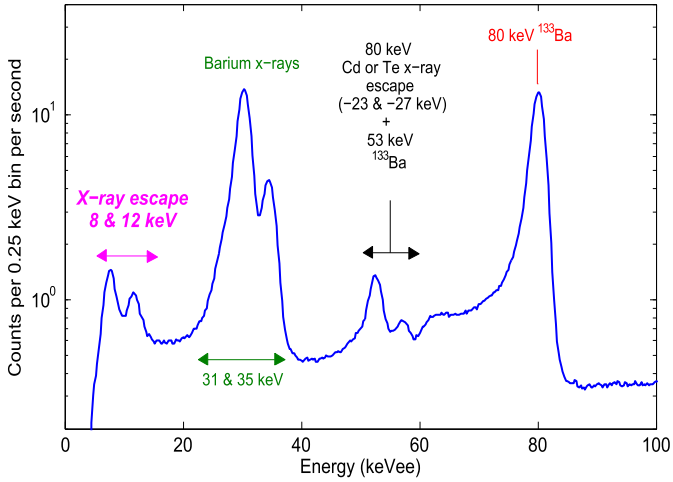

Fig. 6. Recorded energy spectrum from a ^{133}Ba source. Note that X-ray escape produced characteristic peaks at low energies. This measurement lasted 30 min.

the low-energy threshold was developed. A ^{133}Ba source was placed outside the aluminum detector housing. The 31- and 35-keV X-rays produced from the source easily reached the cathode side of the CdZnTe array. Some of these incident X-rays were photoelectrically absorbed and produced a characteristic Cd or Te X-ray that escaped the detection system so that a portion of the deposited energy was not recorded. These events were recorded as escape peaks in the spectrum shown in Fig. 6. The ^{133}Ba X-rays were expected to generate peaks at 4, 8, and 12 keV from these interactions. The peaks at 8 and 12 keV were observed with current thresholds.

IV. Neutron Generator Measurements

As a proof of principle, a Thermo Fisher Scientific MP320 deuterium-deuterium (DD) neutron generator, which produced approximately 10^6 2.5-MeV neutrons per second in 4π, was used to study neutron interactions in CdZnTe detectors. The tube was operated with a potential of 80 kV and a current of 60 μA. The acceleration and deceleration of deuterons produced a significant amount of bremsstrahlung radiation in addition to neutrons. Three millimeters of lead shielding was used to attenuate bremsstrahlung yet preserve neutron signals. The 80-keV emission from a ^{133}Ba source was used to verify that there was ample shielding of bremsstrahlung.

As shown in Fig. 7, a high-energy gamma-ray source can slightly increase the low-energy background level through small-angle Compton scattering events that deposit a small amount of energy in the detector. Yet the increase in counts between 0 and 20 keVee when the neutron generator was producing neutrons is clearly higher than the background level or what can be produced from forward-scttered higher energy photons. Note that the upper end of the low-energy neutron-signature peak begins at around 18 keVee. This indicates a slightly smaller quenching factor, 0.2 rather than 0.25, from the observed to expected (from Fig. 2) backscatter peak position ratio.

Another signature of fast neutron interactions is characteristic gamma rays released from inelastic scattering reactions.

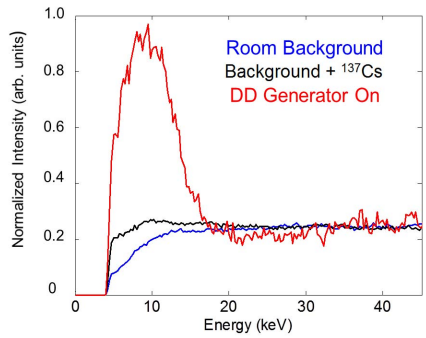

Fig. 7. Recorded energy spectrum from the DD neutron generator compared with background measurements. The spectra are normalized to the count rate in the 30–40-keV range. These spectra also indicate that this neutron detection technique is robust even with a photon source in the background. The ^{137}Cs source was not present during the DD neutron generator measurement. It is included in this figure to demonstrate how forward-scattered gamma-rays can minimally affect the low-energy continuum.

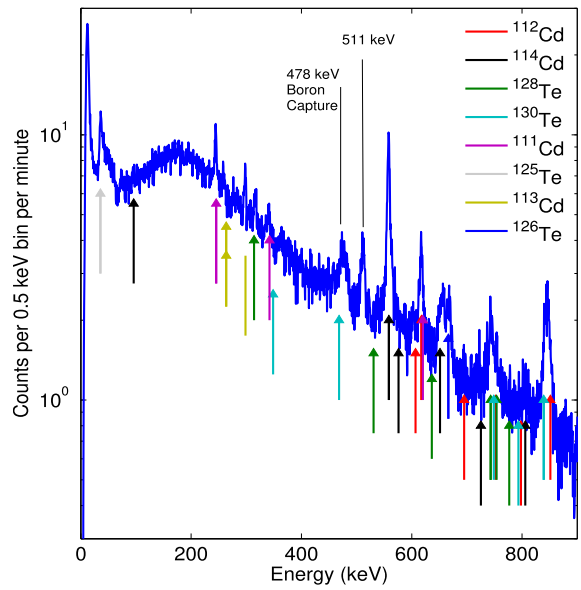

Fig. 8. Recorded background-subtracted energy spectrum from the DD neutron generator zoomed to see high-energy characteristic inelastic scattering gamma rays. Vertical lines are expected inelastic gamma rays from the various constituent nuclei. The 511-keV peak is from pair production of other high-energy gamma rays produced from neutron interactions. The boron capture peak comes from boron in the experimental area as well as boron in circuit board components.

As shown in Fig. 8, the background-subtracted spectra from the system with the neutron generator ON show characteristic peaks related to the constituent isotopes. These signatures may also be used to identify the presence of a neutron source.

To verify that the low-energy signals from 5–20 keVee were from neutrons rather than photons, several techniques were used to isolate the source of this signal. First, the interaction positions of these energy depositions were noted by mapping the small-energy deposition count rate by the triggered pixel location for the neutron irradiation directions shown in Fig. 9. Low-energy photons should either be attenuated by the aluminum detector housing or absorbed on the surface of the CdZnTe. However, as shown in the right window of Fig. 10, when the neutrons are incident from the side of the detector, a substantial number of low-energy events penetrate deep into

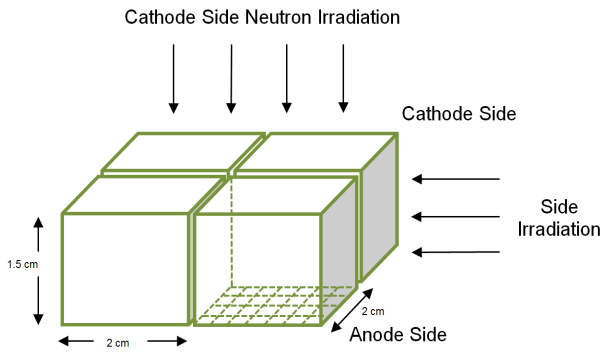

Fig. 9. Sketch of neutron irradiation directions. The gap between detectors is 2 mm.

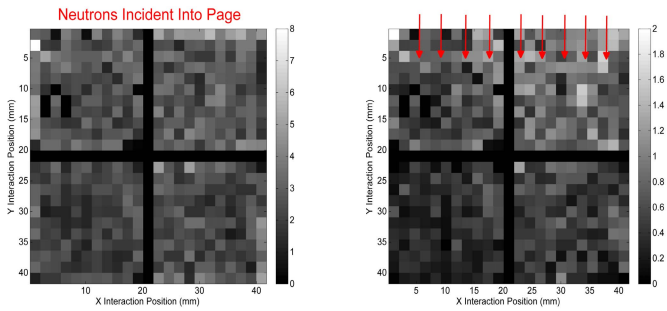

Fig. 10. Background-subtracted count rate (counts per second) for recorded interactions with energy between 0 and 25 keVee for neutrons incident from the cathode side (left) and from the side of the detector array (right).

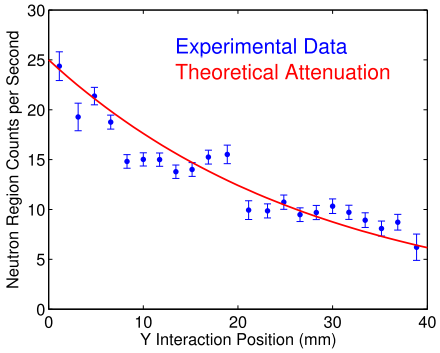

Fig. 11. Number of recorded background-subtracted small-energy depositions as a function of distance into the CdZnTe detector from the right pane of Fig. 10 with the air gap between detectors subtracted. The experimental attenuation matches the theoretical attenuation for neutrons in CdZnTe.

the detector. High-energy photons that are Compton scattered through a small angle have a more uniform interaction position distribution than observed in Fig. 10. In fact, the attenuation of neutrons from this measurement matches the theoretical attenuation of CdZnTe quite well as shown in Fig. 11. The number of counts was calculated by summing the number of counts in each row from Fig. 10 and using the center of the pixel as the average interaction location. Similar results were achieved for neutron irradiations from the other sides, as well as intermediate angles.

Borated polyethylene was placed between the detector array and the neutron generator as seen in Fig. 12. The borated polyethylene should reduce the intensity of fast neutron signatures while allowing transport of higher energy photons. The resulting spectra are shown in Fig. 13. Note that the addition

Fig. 12. Experimental apparatus with CdZnTe array inside black Pelican® case, lavender sheets of borated polyethylene, and the neutron generator tube behind. The metallic shielding was used to eliminate bremsstrahlung.

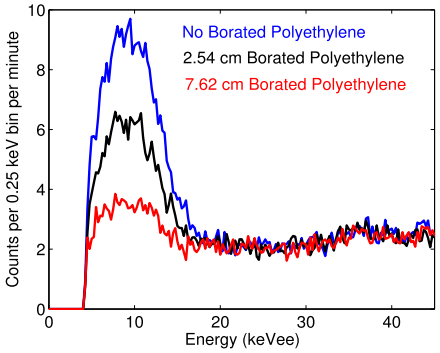

Fig. 13. Recorded energy spectrum from the DD neutron generator with different thicknesses of borated polyethylene moderator between the detector array and the generator.

of polyethylene significantly reduces the relative height of the low-energy peak indicative of fast neutron elastic scattering interactions. One can model the attenuation of neutrons via an exponential factor as

$$\frac{I}{I_0} \approx e^{-\Sigma_t x} \tag{3}$$

where I is the neutron intensity after passing through a moderator with thickness x, I_0 is the initial neutron intensity, and Σ_t is the measured effective attenuation cross section. Equation (3) assumes that neutrons are removed following a single interaction. Multiple detectable scatters are unlikely, so (3) can be used to estimate the neutron attenuation from the borated polyethylene.

Using the net counts (subtracting the mean continuum to the right of the peak) in the neutron signature peak, the measured effective attenuation cross section of the borated polyethylene was calculated to be 0.21 ± 0.05 cm^{-1}. Using MCNPX [25] to simulate the measurement, the effective cross section was calculated to be 0.19 ± 0.01 cm^{-1} using a quenching factor of 25%. Contrastingly, 99% of 10-keV photons would be attenuated by 7.5 cm of polyethylene. High-energy photons do not produce the characteristic peak as shown in Fig. 7. Furthermore, only 1% of 100-keV photons would be absorbed by 7.5 cm of polyethylene. Thus, adding polyethylene between the DD generator and detector array modulates the hypothesized neutron signature peak as incident neutrons

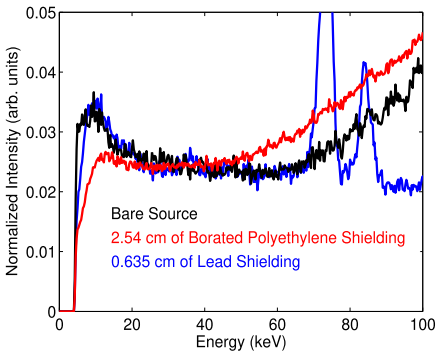

Fig. 14. Recorded energy spectra from a ^{252}Cf source with different moderators between the detector array and the source. The spectra are normalized to the count rate in the 30–40-keV range. Each measurement lasted at least 90 min and each spectra has more than 500-K events between 0 and 400 keV.

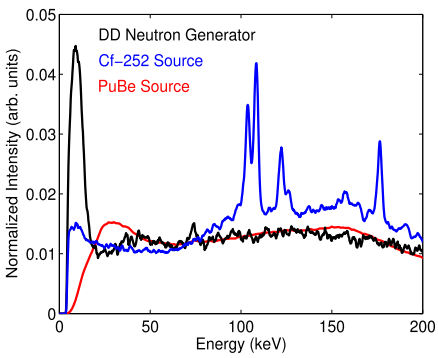

Fig. 15. Recorded energy spectra from a ^{252}Cf spontaneous fission neutron source, a DD neutron generator, and a PuBe (α,n) source. The spectra are normalized to the count rate in the 65–85-keV range.

would, and the spectra cannot be explained by assuming that the interactions are from low-energy or high-energy photons. Therefore, these events must be neutron-induced.

V. Measurements of Nonmonoenergetic Neutron Sources

Realistic neutron sources encountered in the field are not monoenergetic. Rather, they are sources that emit neutrons via fission or (α, n) reactions. A 18 μCi ^{252}Cf spontaneous fission neutron source (generating 80 000 neutrons per second in 4π) was placed 20 cm away from the detector array. Again, some moderating materials were placed between the source and detector array. The recorded energy spectra are shown in Fig. 14. In the cases where the source was bare or shielded with lead, there are considerably more events in the spectra with energy less than 25 keVee, indicating the presence of a neutron source. Note that the lead shield attenuates photon signatures of the material, but the neutron signatures still indicate the possible presence of SNM. Practically, if a plutonium source is adequately shielded with lead, the gamma-ray lines around 400 keV may be attenuated while neutrons pass through the shield; in this case, neutrons provide the only available signal for detection.

Different neutron sources have different energy spectra. Therefore, one would expect the rising portion of the low-energy neutron-signature peak to vary with neutron sources. As shown in Fig. 15, the rising edge of the low-energy peak does change with the neutron source. The PuBe source has the highest neutron energy, so the rising edge begins around 50 keVee. The DD neutron generator is a mono-energetic source, so it has a sharp rising edge, whereas the ^{252}Cf source (a Watt neutron energy distribution) rises more slowly. This observation matches the expected physics of fast neutron detection using elastic scattering interactions in CdZnTe.

VI. Conclusion

High-resolution room-temperature imaging gamma-ray spectrometers are readily deployable in under five minutes. These instruments are able to provide high-resolution gamma-ray spectroscopy (<0.7% FWHM at 662 keV) and gamma-ray imaging through Compton or coded-aperture reconstruction techniques. By adding neutron detection in the same instrument, complementary information about SNM can be ascertained, which is very valuable when a source is shielded with high-Z material. The detection efficiency was estimated to be of the order of a few percent. Photons and neutrons cannot be discriminated on an event-by-event basis, but the aggregate information provided by small-energy depositions plus detected photons following inelastic neutron scattering can be valuable.

To achieve direct fast neutron detection, the low-energy threshold must be lowered below 10 keVee due to the large constituent nuclei in CdZnTe and quenching. Characteristic fast neutron signature small-energy depositions were observed using a DD neutron generator, a weak spontaneous fission source, and an (α, n) neutron source. The neutron signature peak varied with irradiation direction and shielding. Furthermore, different neutron sources produced different peak shapes in agreement with the scattering physics.

Acknowledgment

The authors would like to thank the students and administrators of the Neutron Science Laboratory at the University of Michigan and to Prof. I. Jovanovic, Dr. M. Sharma, and J. Nattress, who were very helpful in providing access to the MP320 DD neutron generator as well as providing training for its use. They would also like to thank the Detection for Nuclear Nonproliferation Group at the University of Michigan for providing access and training to their sources and Prof. S. Pozzi, Dr. S. Clarke, Dr. A. Di Fulvio, and T. Shin, who provided assistance that contributed to the findings in this paper. Any opinion, findings, and conclusions or recommendations expressed in this material are those of the authors and do not necessarily reflect the views of the Defense Threat Reduction Agency or the National Science Foundation.

References

[1] D. Reilly, N. Ensslin, H. Smith, and S. Kreiner, "Passive nondestructive assay of nuclear materials," Los Alamos Nat. Lab., NM, USA, Tech. Rep. NUREG/CR-5550 LA-UR-90-732, 1991.

[2] M. Yamashita, L. D. Stephens, and H. W. Patterson, "Cosmic-ray-produced neutrons at ground level: Neutron production rate and flux distribution," *J. Geophys. Res.*, vol. 71, no. 16, pp. 3817–3827, 1966.

[3] M. Korun, R. Martincic, B. Pucelj, and M. Ravnik, "Sub-pixel position sensing for pixelated, 3-D position sensitive, wide band-gap, semiconductor, gamma-ray detectors," in *Proc. Symp. Radiat. Protection Neighboring Countries Central Eur.*, 1995, p. 116.

[4] A. Miyake, T. Nishioka, S. Singh, H. Morii, H. Mimura, and T. Aoki, "Development of a CdTe thermal neutron detector for neutron imaging," *Nucl. Instrum. Methods Phys. Res. A, Accel. Spectrom. Detect. Assoc. Equip.*, vol. 677, pp. 41–44, Sep. 2012.

[5] D. McGregor, J. Lindsay, and R. Olsen, "Thermal neutron detection with cadmium$_{1-x}$ zinc$_x$ telluride semiconductor detectors," *Nucl. Instrum. Methods Phys. Res. A, Accel. Spectrom. Detect. Assoc. Equip.*, vol. 381, no. 2, pp. 498–501, 1996.

[6] S. T. Brown, Y. A. Boucher, J. Mann, Y. Zhu, and Z. He, "Thermal neutron source location using a 3-D position-sensitive CdZnTe detector array," in *Proc. IEEE Nucl. Sci. Symp. Med. Imag. Conf. (NSS/MIC)*, Oct. 2013, pp. 1–5.

[7] N. Mascarenhas, J. Brennan, K. Krenz, P. Marleau, and S. Mrowka, "Results with the neutron scatter camera," *IEEE Trans. Nucl. Sci.*, vol. 56, no. 3, pp. 1269–1273, Jun. 2009.

[8] F. Brooks, "A scintillation counter with neutron and gamma-ray discriminators," *Nucl. Instrum. Methods Phys. Res. A, Accel. Spectrom. Detect. Assoc. Equip.*, vol. 4, no. 3, pp. 151–163, 1959.

[9] H. Klein and S. Neumann, "Neutron and photon spectrometry with liquid scintillation detectors in mixed fields," *Nucl. Instrum. Methods Phys. Res. A, Accel. Spectrom. Detect. Assoc. Equip.*, vol. 476, nos. 1–2, pp. 132–142, 2002.

[10] J. Ljungvall and J. Nyberg, "A study of fast neutron interactions in high-purity germanium detectors," *Nucl. Instrum. Methods Phys. Res. A, Accel. Spectrom. Detect. Assoc. Equip.*, vol. 546, no. 3, pp. 553–573, 2005.

[11] N. Veselinović *et al.*, "Some peculiarities of digital gamma-ray spectroscopy with germanium detectors performed in presence of neutrons," *Phys. Procedia*, vol. 59, pp. 63–70, Apr. 2014.

[12] M. Streicher, S. Brown, Y. Zhu, D. Goodman, and Z. He, "Special nuclear material characterization using digital 3-D position sensitive CdZnTe detectors and high purity germanium spectrometers," *IEEE Trans. Nucl. Sci.*, vol. 63, no. 5, pp. 2649–2656, Oct. 2016.

[13] M. Streicher, D. Goodman, S. Brown, Y. Zhu, and Z. He, "A method to estimate the atomic number and mass thickness of intervening materials in uranium and plutonium gamma-ray spectroscopy measurements," *IEEE Trans. Nucl. Sci.*, vol. 63, no. 5, pp. 2639–2648, Oct. 2016.

[14] Y. Zhu and Z. He, "Performance of a 2-keV digitizer ASIC for 3-D position-sensitive pixelated semiconductor detectors," in *Proc. IEEE Nucl. Sci. Symp. Med. Imag. Conf. (NSS/MIC)*, Oct. 2012, pp. 4109–4112.

[15] M. Streicher *et al.*, "A portable 2×2 digital 3-D CZT imaging spectrometer system," in *Proc. IEEE Nucl. Sci. Symp. Med. Imag. Conf. (NSS/MIC)*, Nov. 2014, pp. 1–3.

[16] G. F. Knoll, *Radiation Detection and Measurement*. Hoboken, NJ, USA: Wiley, 2000.

[17] J. J. Duderstadt and L. J. Hamilton, *Nuclear Reactor Analysis*. New York, NY, USA: Wiley, 1976.

[18] E. L. Haines and A. B. Whitehead, "Pulse height defect and energy dispersion in semiconductor detectors," *Rev. Sci. Instrum.*, vol. 37, no. 2, pp. 190–194, 1966.

[19] P. Sorensen, "Atomic limits in the search for galactic dark matter," *Phys. Rev. D, Part. Fields*, vol. 91, p. 083509, Apr. 2015.

[20] T. Shutt *et al.*, "Measurement of ionization and phonon production by nuclear recoils in a 60 g crystal of germanium at 25 mK," *Phys. Rev. Lett.*, vol. 69, no. 24, pp. 3425–3427, 1992.

[21] I. Lazanu and S. Lazanu, "Contribution of the electron—Phonon interaction to Lindhard energy partition at low energy in Ge and Si detectors for astroparticle physics applications," *Astroparticle Phys.*, vol. 75, pp. 44–54, Sep. 2016.

[22] S. Agostinelli, "Geant4—A simulation toolkit," *Nucl. Instrum. Methods Phys. Res. A, Accel. Spectrom. Detect. Assoc. Equip.*, vol. 506, no. 3, pp. 250–303, 2003.

[23] Y. Zhu, S. Anderson, and Z. He, "Sub-pixel position sensing for pixelated, 3-D position sensitive, wide band-gap, semiconductor, gamma-ray detectors," *IEEE Trans. Nucl. Sci.*, vol. 58, no. 3, pp. 1400–1409, Mar. 2011.

[24] Z. He, "Review of the Shockley–Ramo theorem and its application in semiconductor gamma-ray detectors," *Nucl. Instrum. Methods Phys. Res. A, Accel. Spectrom. Detect. Assoc. Equip.*, vol. 463, nos. 1–2, pp. 250–267, 2001.

[25] L. S. Waters, "MCNPX user's manual," Los Alamos Nat. Lab., NM, USA, Tech. Rep. LA-UR-02-2607, 2002.